









Article

Coating of Hemp Fibres with Hydrophobic Compounds Extracted from Pine Bark

Robert Abbel ^{1,*} , Regis Risani ¹, Maxime Nourtier ¹, Lloyd Donaldson ¹ , Christel Brunchwitz ¹, Claire Mayer-Laigle ² , James H. Bridson ¹ , Armin Thumm ¹, Alan Dickson ¹ , Rachel Murray ¹ , Jessica Harris ¹, Johnny Beaugrand ³  and Stefan Hill ¹ 

¹ Scion, Rotorua 3046, New Zealand; stefan.hill@scionresearch.com (S.H.)

² National Research Institute for Agriculture, Food and the Environment (INRAE), 34060 Montpellier, France; claire.mayer@inrae.fr

³ National Research Institute for Agriculture, Food and the Environment (INRAE), 44316 Nantes, France; johnny.beaugrand@inrae.fr

* Correspondence: robert.abel@scionresearch.com

Abstract: Applying coatings of paraffins and other synthetic waxes is a common approach to impart hydrophobic properties to fibres and thus control their surface characteristics. Replacing these fossil-based products with alternatives derived from renewable resources can contribute to humankind's transition to a sustainable bioeconomy. This study presents the coating of hemp fibres with waxes extracted from pine bark as an exemplar application. Two bio-based emulsifiers were used to prepare wax emulsions suitable for a dry blending process. The coatings on the fibres were characterised, quantified, and visualised using a combination of spectroscopic and microscopic techniques. Confocal fluorescence microscopy was an excellent tool to investigate the spatial distribution of the pine bark waxes on the fibre surfaces. While successful deposition was demonstrated for all tested formulations, coating homogeneity varied for different emulsifiers. Compounding the hemp fibres with a bio-based polyester resulted in the substantial improvement of the mechanical behaviour. However, the presence of a wax coating on the fibres did not lead to a significant change in mechanical properties compared to the controls with uncoated fibres. Optimising the composite chemistry or adjusting the processing conditions might improve the compatibility of the hemp fibres with the matrix material, resulting in enhanced mechanical performance.

Keywords: hemp fibres; hydrophobic coatings; pine bark waxes; natural fibres; fibre-reinforced composites; bio-based composites



Citation: Abbel, R.; Risani, R.; Nourtier, M.; Donaldson, L.; Brunchwitz, C.; Mayer-Laigle, C.; Bridson, J.H.; Thumm, A.; Dickson, A.; Murray, R.; et al. Coating of Hemp Fibres with Hydrophobic Compounds Extracted from Pine Bark. *Fibers* **2024**, *12*, 96. <https://doi.org/10.3390/fib12110096>

Academic Editor: Vincenzo Fiore

Received: 29 July 2024

Revised: 2 October 2024

Accepted: 25 October 2024

Published: 7 November 2024



Copyright: © 2024 by the authors. Licensee MDPI, Basel, Switzerland. This article is an open access article distributed under the terms and conditions of the Creative Commons Attribution (CC BY) license (<https://creativecommons.org/licenses/by/4.0/>).

1. Introduction

When applied as coatings, paraffin waxes and other fossil-derived hydrophobic (non-polar) substances are excellent products that are able to impart water-repellent properties to a wide variety of materials. A significant application area for these compounds is the surface treatment of natural fibres to enhance their hydrophobicity. Wax-coated natural fibres have been demonstrated as functional components of wound dressings [1], building materials such as cement [2], and functional textiles [3,4]. Another important application area is fibre-reinforced plastic composites. Due to their hydrophilic nature, compounding natural fibres with polymers often results in composites that are sensitive to moisture [5,6]. Another frequently encountered issue in these materials is insufficient compatibility between the hydrophilic fibres and the hydrophobic polymer matrix [6–8]. This can lead to poor interfacial adhesion which in turn reduces the ability for stress transfer between the composite components. Ultimately, the result is an unsatisfactory mechanical performance. A common approach to improve the compatibility between natural fibres and non-polar polymer matrices in composites is to coat the fibres with paraffins and other waxes. For example, Nhlapo and Luyt co-extruded low-density polyethylene, sisal fibres,

and paraffin waxes, and showed that the waxes crystallised preferably around the short sisal fibres, which improved the Young's modulus [9]. Very similar results were obtained by Atthikumar et al. who used hemp fibres instead [10].

Bio-based hydrophobic compounds have been used for millennia but have recently attracted renewed attention as sustainable alternatives to fossil-derived products [11,12]. They have the potential to support the establishment of a more sustainable global economy and to reduce humankind's reliance on non-renewable resources such as petroleum. Their use for the surface treatment of bran fibres has been demonstrated to increase the elongation at break for composites prepared with aliphatic biopolyesters [13].

Recently, the barks of several tree species have been identified as rich sources of waxy substances [14–16]. For example, it has been demonstrated that *Pinus radiata* Don (radiata pine or Monterey pine) contains a range of non-polar chemicals, which can be extracted using a variety of methods [16–19]. Radiata pine is commercially grown on more than 4 million hectares worldwide and contributes significantly to the economies of several countries [20]. About 90% of the 1.8 million hectares of plantation forest in New Zealand are covered with *P. radiata* [21]. Given that bark comprises 9–15% of the total volume of a tree, it is one of the most available by-products derived from wood-based industries [22]. Although there is thus a clear potential to obtain natural waxes from pine bark in industrially relevant quantities, their potential as functional coatings has so far hardly been experimentally investigated [23,24].

This study describes the deposition of waxes, extracted from radiata pine bark using supercritical carbon dioxide, onto technical hemp fibres. Hemp (*Cannabis sativa* L.) is an important source of natural fibre which is increasingly being used in a variety of applications [25–27], including the reinforcement of biopolymer composites [28–33]. As an industrial crop, hemp offers multiple benefits, such as great potential for drought resistance [34] and the supply of additional valuable products (oils, proteins) besides fibre [35]. Several studies have described the coating of hemp fibres with waxes. A textile made of a mixture of hemp and cotton fibres has been rendered water-repellent by the application of carnauba wax [4]. Beeswax coatings have been applied to hemp fibres to increase their hydrophobicity for improved stability against alkaline hydrolysis in mortars [2]. Similar studies have also been reported using stearic acid [36] or paraffin waxes [37] instead. Paraffin waxes have also served as compatibilisers for polyethylene and hemp fibres in composite materials [10].

In the present study, two bio-based emulsifiers have been used to stabilise the aqueous wax emulsions: polysorbate (T20) and Spirulina (*Arthrospira platensis* Gomont; Sp). T20 is a non-ionic surfactant derived from sorbitol and fatty acids [38] and Sp is the biomass of cyanobacteria, the main components of which are proteins [39]. T20 was chosen because it has been proven highly effective in stabilising dispersions of hydrophobic substances in water, both on its own [40] and in combination with other surfactants [41]. Sp was chosen because, in addition to it being effective as an emulsifier [39,42], its photoluminescent properties enable the direct visualisation and analysis of its spatial distribution through fluorescence microscopy [43]. To avoid intensive physical or chemical fibre treatment, a dry blending process was used to coat the natural fibres with the waxes [44]. A combination of microscopic and spectroscopic techniques (FTIR, NMR, fluorescence microscopy) proved highly useful to demonstrate successful wax deposition on the fibres and to visualise the spatial distribution of the wax coatings on the fibres. Both wax-coated and non-treated control fibres were compounded with bio-based and biodegradable poly(butylene succinate) (bPBS) to form fibre reinforced composites derived from renewable resources. This reinforcement resulted in substantial improvements in mechanical performance compared to plain bPBS. However, in the system studied here, no specific beneficial effects of the presence of waxes on the hemp fibres were found. This was likely due to the detachment of the waxes from the fibre surfaces and dissolution in the rather non-polar bPBS matrix. In the future, natural fibres coated with pine bark waxes could exhibit beneficial effects in biocomposites if somewhat more polar matrix polymers such as poly(lactic acid) or other

poly(hydroxy alkanolic acids) with shorter repeat units were used instead [45,46]. Further potential future application areas for pine wax-coated hemp fibres could be in insulation panels [47] or fibrous packaging [48].

2. Materials and Methods

2.1. Materials

Crude pine wax (CPW) was obtained by extracting *P. radiata* bark using supercritical CO₂. The bark was sourced from Bark Products Taranaki (Waitara, New Zealand) and extracted at Pharmalink (Appleby, New Zealand) in a high-pressure system equipped with 850 litre extractor vessels (NATEX, Ternitz, Austria). A total of 679.5 kg of bark was packed into the extraction vessels. Extraction was carried out over 6 h and performed at a temperature of 50 °C and a pressure of 300 bar. The average CO₂ flow rate was 3400 kg/h and the extracts were collected in a separator at 70 bar pressure and 65 °C. Refined pine wax (RPW) was obtained by cold ethanol winterisation from the CPW, following the established literature procedures [49]. Refined yellow beeswax (BW) pellets were purchased from NZ Beeswax Ltd. (Hamilton, New Zealand) and were used as received. Sorbitan ester surfactant Tween20 (T20) was provided by Sigma-Aldrich (Merk Group, St. Louis, MO, USA). Spirulina (Sp) was supplied by Atelier Luma (Arles, France) and ground into a fine powder using an impact milling device (Hosokawa Alpine, Ultraplex UPZ 100, Runcorn, United Kingdom). The grinding process involved three passes, with a screen size of 0.3 mm for the first pass and a screen size of 0.1 mm for the two subsequent passes. The dimensions (volume-weighted diameter, d) of the ground Sp powder (d₁₀, d₅₀, and d₉₀) were measured in ethanol dispersion (2 wt%) using laser diffraction (LS 13 320 XR particle sizer (Beckman & Coulter, Villepinte, France) with a universal liquid module and sonicator. A cuvette was filled with ethanol, sonicated to remove air bubbles, and then the Sp powder was added. Subsequent agitation at 45% of the maximum pump speed and then sonication for two minutes at full power were applied to achieve complete dispersion. Samples were analysed in triplicate. The particle size distribution was characterised by d₁₀ = 3.47 µm, a median size d₅₀ = 16.31 µm, and d₉₀ = 39.64 µm. Technical hemp fibres (Hf) from *C. sativa* with an average length of 1 mm were supplied by FRD (Fibres Recherche Développement, Troyes, France). The fibres have been analysed for their chemical composition with regard to extractables, lignin content, carbohydrate composition, and ash content; the results and methods are reported in the Supplementary Materials (Table S1) and in part also in an earlier publication [50]. Bio-based polybutylene succinate (bPBS) was provided by PTT Mitsubishi Chemical Corporation Biochem Company (trade name BioPBSTM FZ71PM, density: 1.26 g/cm³, melt flow index (190 °C, 2.16 kg): 22 g/10 min).

2.2. Materials Preparation

2.2.1. Emulsion Preparation

Emulsions were prepared using a 1:2 wax-to-water ratio (by weight) and an emulsifier concentration of 5 wt%. The wax (12.6 g) and water (25.3 g) were placed in a glass beaker and heated to 80 °C on a Heidolph hot plate to melt the waxes. Once the wax was completely melted, the emulsifier (2.0 g) was added. Then, the mixture was homogenised using an ultrasonic mixer from OMNI Homogenizer for 3 min at a speed of 10,000 rpm and used immediately after preparation for the dry blending process.

2.2.2. Dry Blending of Fibres and Emulsions

Hemp fibres (400 g) were coated with 40 g of emulsion (10:1 fibre to emulsion ratio) using a dry blending process [44]. The setup consists of a 12 m steel loop (diameter 16 cm) with a fan creating turbulent air flow. The fibres were suspended in an air stream for 3–4 min to break any entanglements, and to separate any bundles into individual fibres. Then, the wax emulsion was added into the air stream using a spray gun. Both the emulsions and the spray gun were kept at approximately 50 °C to keep the waxes in a liquid state and to prevent the clogging of the gun. Prior to each run, boiling water was

circulated through the spray-gun to keep it above the melting temperature of the waxes and to ensure that the wax would not cool down and solidify during the spraying process. Immediately after the wax had been applied, the fibres were ejected into a muslin bag for collection. Each batch of coated fibres was frozen to $-80\text{ }^{\circ}\text{C}$ overnight and then lyophilised for 48 h using an Edwards freeze dryer with an MVP 24 vacuum pump (Woosung Vacuum, Jeju, Republic of Korea).

2.2.3. Compounding

bPBS/Hf composites were prepared using a 26 mm co-rotating twin-screw LabTech LTE26-40 extruder (Labtech Engineering, Phraeksa, Thailand; L/D ratio 40) and two gravimetric feeders (Weighbatch DS10 for the polymer and Coperion K-tron K-ML-SFS-KT20 for the fibres). Feeding rates into the extruder were 5.4 kg/h for the bPBS pellets and 0.6 kg/h for the coated fibres, respectively. The extruder barrel was heated to a temperature profile of $150\text{ }^{\circ}\text{C}$ (feeder and die) to $160\text{ }^{\circ}\text{C}$ (melting and mixing zones) with a screw speed of 160 rpm. The die pressure was 27 bar to achieve a throughput of 6 kg/h. The extruded strands (diameter 3 mm) were cooled in a water bath (ambient temperature) and then cut into 1.5 mm pellets using a Pelletiser CZ-120-SFS-KT20. The pellets were then oven-dried at $60\text{ }^{\circ}\text{C}$ overnight and placed in hermetic sealable bags to prevent water absorption. The composition of the resulting composites is described in Table 1.

Table 1. Description of the fibre/bPBS composites prepared for this study.

Composite	Emulsifier	Wax Type	Coated Hf ⁶ (wt%)	bPBS ⁷ (wt%)
bPBS-Hf-CPW-T20	T20 ¹	CPW ³	10	90
bPBS-Hf-CPW-Sp	Sp ²	CPW	10	90
bPBS-Hf-RPW-T20	T20	RPW ⁴	10	90
bPBS-Hf-RPW-Sp	Sp	RPW	10	90
bPBS-Hf-BW-T20	T20	BW ⁵	10	90
bPBS-Hf-BW-Sp	Sp	BW	10	90
bPBS-Hf-Control	-	-	10	90
bPBS	-	-	0	100

¹ T20: Polysorbate 20; ² Sp: Spirulina; ³ CPW: crude pine bark wax; ⁴ RPW: refined pine bark wax; ⁵ BW: beeswax; ⁶ Hf: hemp fibre; ⁷ bPBS: bio-polybutylene succinate.

2.2.4. Injection Moulding

The compounded pellets were injection moulded using a BOY 35 machine (BOY Spritzgussautomaten, Neustadt-Fernthal, Germany) into ISO multipurpose test specimens type 1A (ISO 527-2 standard [51]). The process parameters that were used are presented in Table 2.

Table 2. Processing conditions used for injection moulding of the fibre/bPBS composites.

Process Parameter	Value(s)
Barrel positions (mm)	66/20/15/10/5/2
Injection pressure (bar)	50
Injection speed (mm/s)	45
Screw speed (rpm)	100
Back pressure (bar)	15
Hold time (s)	3/20
Hold pressure (bar)	60/40
Cooling time	30
Nozzle temperature ($^{\circ}\text{C}$)	160
Barrel temperature ($^{\circ}\text{C}$)	160
Mould temperature ($^{\circ}\text{C}$)	25

2.3. Characterisation

2.3.1. Gas Chromatography—Mass Spectrometry (GC-MS) Analysis of Waxes

Pyridine (50 μL) was added to a solution of wax (1–2 mg) in chloroform (1.0 mL). Then, bis(trimethylsilyl)trifluoroacetamide and trimethylchlorosilane (BSTFA:TMCS, 99:1, 100 μL) were added and the resulting mixture was vortexed and heated (70 $^{\circ}\text{C}$) for 1 h. This procedure transforms alcohol, phenol, and organic acid groups to their respective trimethylsilyl (TMS) derivatives. Samples were analysed quickly after derivatisation; 1 μL of sample solution was injected onto an Agilent 7890B gas chromatograph connected to a 5877B mass spectrometer. An HP-Ultra2 column (L \times I.D. 50 m \times 200 μm , d_f 0.33 μm) served as the stationary phase and ultra-high purity helium (99.999%) served as the mobile phase (flow rate 1 mL \cdot min $^{-1}$). Injection and interface temperatures were 280 $^{\circ}\text{C}$ and 300 $^{\circ}\text{C}$, respectively, and the following temperature program was used: 40 $^{\circ}\text{C}$ start, ramp 6 K \cdot min $^{-1}$ to 300 $^{\circ}\text{C}$, 30 min hold. The temperature of the mass spectrometry source was set to 250 $^{\circ}\text{C}$ and the quadrupole was set to 150 $^{\circ}\text{C}$ (ionisation energy 70 mV). Agilent's Masshunter software (version 10) was used for data analysis. Compound identification was achieved through sequential spectrum matching using the commercial NIST14 mass spectral library. Semi-quantitative analysis was obtained through relative integration of peak areas.

2.3.2. Thermal Testing (Thermogravimetric Analysis (TGA) and Differential Scanning Calorimetry (DSC))

Prior to characterising the thermal behaviour of the wax emulsions, each emulsion was dried in a vacuum oven at 24 $^{\circ}\text{C}$ for approximately 12 h. The thermal degradation behaviour of the materials was studied using a Discovery TGA (TA Instruments, New Castle, DE, USA). The samples (c.a. 10 mg) were transferred into platinum HT sample pans (TA Instruments, 100 μL) and heated from ambient temperature to 500 $^{\circ}\text{C}$ at a heating rate of 10 K \cdot min $^{-1}$ under a nitrogen atmosphere (10 mL \cdot min $^{-1}$). All of the samples were analysed in triplicate. TGA weight calibration was carried out using a calibration pan with a known weight; temperature calibration was performed using calcium oxalate.

Calorimetric experiments were performed with a Discovery differential scanning calorimeter (TA Instruments, New Castle, DE, USA). Composite samples were prepared by cutting a transverse section from the central part of a tensile specimen (to avoid skin effects on the crystallinity). Starting materials and emulsions were analysed 'as is'. Samples (ca. 5 mg) were accurately weighed into TZero aluminium pans and analysed using a heat-cool-heat programme (Supplementary Materials, Table S2) at 10 K \cdot min $^{-1}$ under a nitrogen atmosphere (50 mL \cdot min $^{-1}$). All experiments were run in triplicate. The DSC calibrations of temperature and heat flow were performed using an indium metal standard.

The degree of crystallinity (X_c) of bPBS in the composites was estimated using Equation (1):

$$X_c = \frac{\Delta H_m}{\Delta H_m^{\circ} (1 - W_f)} \times 100 \quad (1)$$

where ΔH_m is the measured melting enthalpy of the crystalline bPBS fraction, W_f the fibre weight fraction in the composite, and ΔH_m° the theoretical melting enthalpy of fully crystalline PBS (200 J/g [52,53]).

2.3.3. Fourier Transform Infrared (FTIR) and Nuclear Magnetic Resonance (NMR) Spectroscopies

FTIR spectra were acquired using a Bruker Tensor 27 instrument fitted with a Bruker Platinum attenuated total reflectance (ATR) accessory (Diamond cell). Spectra were acquired with 32 background and sample scans between 4000 cm^{-1} and 400 cm^{-1} at 4 cm^{-1} resolution. Each formulation was analysed in triplicate. Baseline correction and normalisation (rubberband method, 128 baseline points, carbon dioxide band excluded) were performed using Bruker OPUS software (version 8.2).

Solid-state ^{13}C NMR was performed using a 200 MHz Bruker NMR spectrometer fitted with a 4 mm MAS probe and analysed using Cross-Polarisation Magic Angle Spinning (CP-MAS) at a rate of 5 kHz. The pulse program that was employed was a standard cross-polarisation experiment, with a pulse delay of 1.5 s, a proton preparation pulse of 3.5 μs , a contact time of 1 ms, and an acquisition time of 26 ms. Then, 10 k pulses were applied, the resulting signals were Fourier-transformed with a Gaussian broadening of 25 Hz, and then they were phase-adjusted and integrated using the Bruker TopSpin software (version 3.6.5). All spectra were internally calibrated to the domain-1/interior C4 signal of cellulose at 89 ppm. For wax quantification, the spectral region between 0 and 45 ppm was integrated, and for cellulose, the region between 45 and 150 ppm was integrated.

2.3.4. Water Contact Angle Measurements

The fibres were dispersed into a slurry with water, then dewatered using a filter paper and a Büchner funnel. The surface of the resultant fibre pad was analysed using an FTA1000 Dynamic Contact Angle Analyser (First Ten Angstroms, Portsmouth, VA, USA) with deionised water as the test liquid.

2.3.5. Microscopy

A Leica SP5 confocal microscope was used to carry out the fluorescence imaging using UV and visible excitation. The fibre samples were mounted in pH 9 buffer to enhance fluorescence. Excitation was conducted at 355, 488, and 561 nm. Emission was measured at 400–480 nm, 500–550, and 570–700 nm, respectively. Images were rendered as maximum-intensity projections. Fluorescence spectra for the wax samples and for Sp were acquired using either UV (355 nm) or green (561 nm) excitation.

All SEM analyses were imaged using a JEOL 6700 Field Emission Scanning Electron Microscope (JEOL Ltd., Tokyo, Japan). Samples were mounted on stubs using carbon adhesive tape, sputter coated with 10 nm platinum and imaged using an accelerating voltage of 3.0 kV with a lower secondary electron (LEI) detector.

2.3.6. Mechanical Testing

Prior to mechanical testing, the samples were conditioned at 23 °C and 50% \pm 10% relative humidity (RH) for at least 48 h. Samples for tensile, flexural, and impact testing were cut out from the injection moulded material using a band saw, at dimensions as specified by the relevant standards (Tensile: ISO 527-2 standard [51]; Flexural: ASTM D790-17 standard [54]; Impact: ISO 180 standard [55]). The tensile and flexural characterisation was performed with a universal material testing machine (Instron 5982; Norwood, MA, USA) operating in traction and compression modes, respectively, and using a 10 kN load cell. Five specimens were tested for each composite. The software used was Bluehill Universal 4.08. Young's moduli were obtained at a test speed of 1 mm·min⁻¹ from 0.0 to 0.4% deformation. Beyond 0.4% deformation, 50 mm·min⁻¹ test speed was applied to obtain maximum strain and maximum stress. A video extensometer was used to monitor the deformation strain. A 0.5 N preload was applied at the beginning of the test to remove any slack in the specimen prior to recording. For flexural three-point bending tests, the crosshead motion was set to 2 mm·min⁻¹ between the spans with span radii of 64 mm. For the impact specimens, the pieces were notched, i.e., a pre-cut to the standard dimensions was made. Testing was carried out on a Ceast Resil Impactor (P/N 6957.000, Instron, Norwood, MA, USA). The hammer that was used had a maximum impact energy of 0.5 J. A minimum of ten replicates were tested for each composite.

3. Results and Discussions

3.1. Characterisation of Starting Materials

Crude pine wax (CPW) was extracted from *P. radiata* bark using supercritical CO₂ with a yield of 2.5 wt%, and its composition was analysed using GC-MS. The main chemical classes identified included fatty acids and resin acids (20–30% each), with minor fractions

of fatty alcohols and phytosterols (<10%). Winterisation (recrystallisation from absolute alcohol at low temperatures [49]) resulted in a refined pine wax (RPW) with an enhanced content of aliphatic molecules, while resin acids and phytosterols were significantly reduced. Beeswax (BW) was also included in this study as a reference material [2,56]. Its chemical composition is known from the literature and differed considerably from both types of pine bark wax. Although bee genetics and diet can cause some variations, it typically contains significant amounts of hydrocarbons, linear wax monoesters and hydroxymonoesters, and complex wax esters, none of which were detected in either CPW or RPW [57]. By contrast, free fatty acids are only a minor constituent of BW [12,57]. The chemical analysis of the hemp fibres used in this study revealed that they contained about 0.5 wt% extractives, 5.5–5.8 wt% lignin, 77–81 wt% carbohydrates (the vast majority of which (68–70 wt%) composed of glucosyl units), and about 1.7 wt% ash. These findings are consistent with results published earlier by some of the authors of this study [50] and also with the findings reported in other publications [58]. Two commercially available bio-based emulsifiers (polysorbate (T20) and Spirulina (Sp)) were tested in this work, to understand their influence on the spraying process and on the quality of the wax coatings deposited on the natural fibres.

The thermal stability and degradation behaviour of the starting materials were studied using thermogravimetric analysis (TGA) to ensure they did not undergo substantial degradation under the conditions applied during emulsion preparation and downstream processing (maximum temperature 160 °C). Figure 1a displays the thermal degradation of the neat waxes (CPW, RPW and BW) and the emulsifiers (T20 and Sp). All TGA data, except those for BW, showed a mass loss below 100 °C, corresponding to the evaporation of water present in the materials. The absence of this phenomenon for BW indicates that it has a stronger hydrophobic character than the pine bark waxes and therefore does not absorb significant amounts of water. This finding is in line with the known composition of BW, which is very low in components with polar functional groups such as alcohols or carboxylic acids, rendering it with a stronger hydrophobic nature. The water contents of both types of pine wax were similar, in the range of 1.5–2.0%. Only very minor differences in degradation behaviour were observed between CPW and RPW, indicating that the winterisation process had no major influence on their thermal stabilities. Both waxes were stable up to about 200 °C, demonstrating that they could withstand downstream processing conditions. BW started to degrade at significantly higher temperatures (beyond 250 °C), in line with what has been reported earlier in the literature [56]. The increased thermal stability of the BW can be explained by its chemical composition, which contains a higher proportion of long-chain aliphatic (i.e., less volatile) components than either of the pine waxes [12,57].

The two emulsifiers exhibited very different thermal stabilities. Sp exhibited a higher water content (7.7%) than T20 (1.9%), as evidenced by the mass loss below 100 °C. No significant further mass loss was observed for either of the emulsifiers until up to at least 180 °C, demonstrating, as with the waxes, that no thermal degradation issues were to be expected during downstream processing. At 500 °C, Sp had only degraded by 60% of its original weight, while T20 had lost 97% of its mass. A similar Sp degradation pattern has been reported earlier by Larrosa et al. [59].

The DSC characterisation of the waxes (Figure 1b) revealed a generally similar overall pattern with a melting peak between 55 and 65 °C, and a corresponding crystallisation peak upon cooling. CPW differed from RPW in both a lower transition temperature (by ca. 10 °C) and a smaller enthalpy of melting (by ca. a factor 2), indicating a lower degree of structural order (crystallinity) in the CPW. This observation is in line with the higher purity of the RPW and also with the chemical nature of its main composition; linear saturated aliphatic molecules are more prone to crystallisation than the more structurally irregular resin acids [60]. In addition, a second, weaker transition at lower temperatures was more pronounced in RPW compared with CPW. This indicates the enrichment through the winterisation process of a second class of wax components which form a second phase with

lower thermal stability. Fatty alcohols which tend to melt at a lower temperature than carboxylic acids with the same chain length [61] or a small fraction of shorter chain molecules are possible candidates, but further research is required to confirm this working hypothesis. BW showed a more complex phase behaviour with even more pronounced melting and crystallisation peaks that were clearly composed of several overlapping transition processes, in line with earlier findings reported by other authors [56].

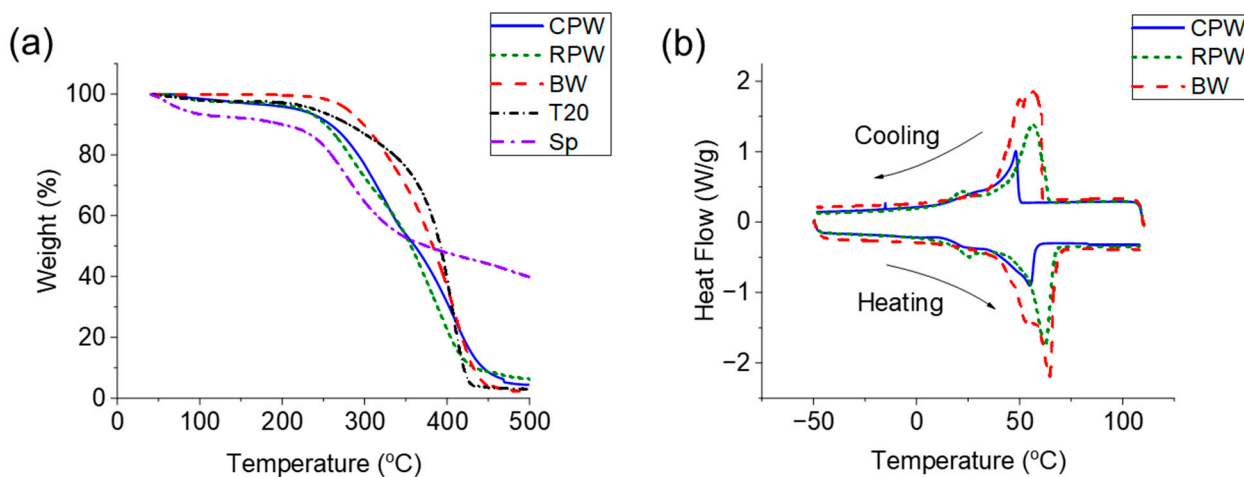


Figure 1. Thermal properties of starting materials. (a) Thermal degradation behaviour (determined by TGA) of the pure waxes (CPW, RPW and BW) and emulsifiers (T20 and Sp). (b) Phase behaviour (determined by DSC) of the pure waxes (cooling run and second heating run; exo up).

3.2. Water/Wax Emulsions

Emulsions were prepared by homogenising water/wax/emulsifier mixtures at temperatures above the melting point of the waxes and were characterised thermally to determine if they were stable during the extrusion and injection moulding processes. The thermal degradation behaviour of the emulsions' solid content (i.e., after drying) is displayed in Figure 2a. All materials showed indications for three distinct degradation processes occurring at different temperatures, although overlap in the temperature ranges made it challenging to clearly separate them from each other. The presence of these processes was more clearly evident in a plot of the derivative of weight vs. temperature, which is displayed as an exemplar for CPW-T20 and CPW-Sp in Figure 2b. In contrast to the pure pine waxes (Figure 1a), their emulsions did not show a significant weight loss below 100 °C, indicating that the drying procedure had effectively removed any moisture content. All emulsions were stable until at least 200 °C, demonstrating their ability to withstand the processing conditions for the extrusion of the bPBS matrix (maximum 160 °C; illustrated by the dotted line). For all emulsions, the first significant thermal degradation step started at around 260–265 °C (Supplementary Materials, Table S3). No significant effects of the individual waxes or emulsifiers on the thermal stabilities of the emulsions could be detected.

For all tested formulations, more than 80% of the organic matter had disappeared at the end of the degradation processes. The degradation behaviour at high temperatures was largely determined by the emulsifier used. Regardless of the wax type, emulsions with Sp displayed a distinct shoulder between 400 and 500 °C, resulting in a lower final (at 500 °C) weight loss than the corresponding T20-based formulations. This finding aligns with the degradation characteristics of pure Sp observed in Figure 1a, as highlighted in the previous paragraph.

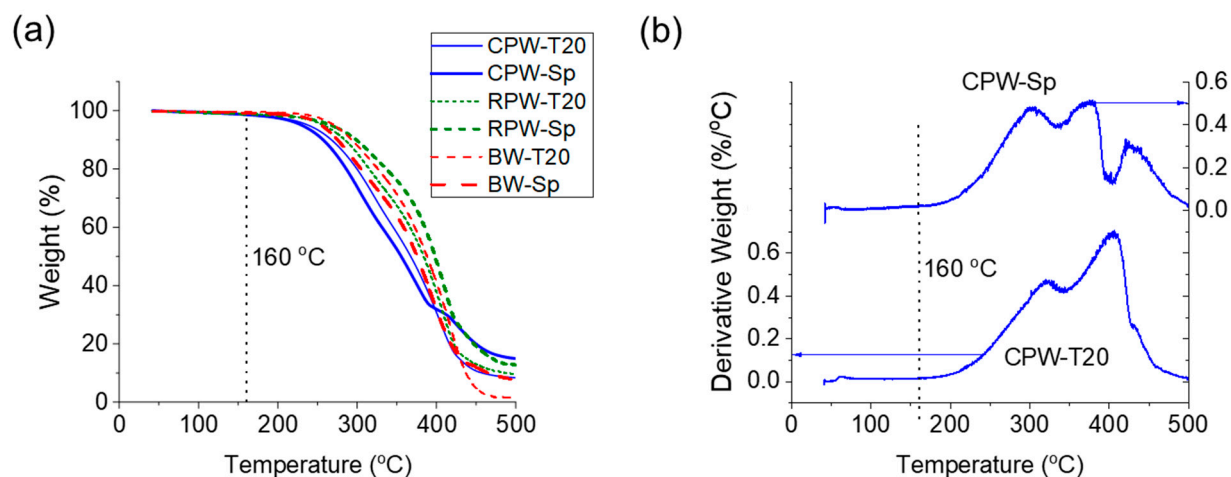


Figure 2. Thermal degradation behaviour of dried wax emulsions. (a) TGA thermogram showing the different degradation steps for the emulsions. (b) Exemplar derivative weight as a function of temperature for the two CPW formulations; for clarity, the scale is offset between both emulsions. The dotted line at 160 °C indicates the maximum temperature of downstream processing.

DSC traces for all emulsions are shown in the Supplementary Materials (Figures S1–S3), and the most important parameters are summarised in Table 3. Due to the better control over thermal history, the data from the second heat ramp were used to compare the melting enthalpies of the different emulsions and to determine the influence of the wax type on their phase behaviours. Generally, the trend in melting enthalpies (and therefore likely levels of crystallinity) followed that of the pure waxes: all CPW emulsions had lower values than RPW emulsion, and these were again lower than for BW. Quantitative differences were substantial between the individual groups of materials containing the same waxes. The crystallisation behaviour of the base waxes is therefore clearly the governing factor for the thermal properties of the emulsions. However, more subtle differences were induced by the nature of the emulsifiers, too. All Sp emulsions had higher melting enthalpies than emulsions prepared using T20, regardless of the wax used. These differences can be explained by the nature of the emulsifier: Sp, as a powder, acts as a nucleating agent in contact with the waxes, in a similar way that Shi et al. demonstrated for different types of biomass particulates [62]. By contrast, T20, being a small molecule, is likely unable to induce or enhance crystallisation. A comparison of the pure waxes with the emulsions showed that the addition of emulsifier increased the crystallinity of CPW, while it decreased that of both RPW and BW. By contrast, there were no major differences in peak position (temperature of the peak maximum) for either melting or crystallisation transitions, indicating that the emulsifiers likely affected only the extent of the crystallisation, but not the internal structure of the crystalline domains.

Table 3. Thermal characteristics (determined by DSC; results from second heat ramp) of neat waxes and dried emulsions. Experimental uncertainties are reported as one standard deviation ($n = 3$).

	Melting Enthalpy (J/g)	Peak Maximum (°C)
CPW	60.1 ± 1.3	50.6 ± 0.1
CPW-T20	61.6 ± 2.5	54.4 ± 0.1
CPW-Sp	68.0 ± 0.2	48.7 ± 0.1
RPW	130.6 ± 0.4	57.4 ± 2.8
RPW-T20	106.7 ± 1.9	61.5 ± 0.1
RPW-Sp	122.5 ± 0.4	59.8 ± 0.3
BW	171.6 ± 0.8	64.2 ± 0.1
BW-T20	138.7 ± 4.1	63.8 ± 0.2
BW-Sp	153.5 ± 0.9	63.6 ± 0.2

3.3. Dry Blending Process

A dry blending process was employed to deposit the wax emulsions on the hemp fibres [44]. The emulsions were dosed in such a way that resulted in a wax content of 2–3 wt% on the fibres. FTIR spectroscopy was used to qualitatively confirm the presence and relative concentrations of waxes on the fibres after the coating process. The spectra of the neat waxes exhibited a strong CH stretching vibration ($2800\text{--}3000\text{ cm}^{-1}$), as well as carbonyl stretching vibrations ($1700\text{--}1740\text{ cm}^{-1}$) and CH_2 bending vibrations (1450 cm^{-1}), consistent with the presence of fatty acids and their esters, resin acids, and other saturated hydrocarbons (Supplementary Materials; Figure S4). The presence of these components is in line with the results obtained by GC-MS and with the literature on BW composition. After fibre coating, an increase in the CH stretching vibration was observed for all formulations, clearly indicating the presence of waxes (Figure 3; Supplementary Materials, Figure S4). A small increase in the band at 1740 cm^{-1} in the wax-coated fibres with T20 emulsions is probably due to the ester bonds in T20. Replicates between different samples prepared using the same conditions showed high reproducibility, indicating a good wax-in-water dispersion and a homogeneous distribution of the emulsions on the fibres during the spraying process, resulting in a uniform coating on a macroscopic level. According to the FTIR spectra, both CPW and RPW consistently showed a higher load of waxes when T20, rather than Sp, was used as the emulsifier. By contrast, BW deposition was more efficient starting from a Sp-based emulsion. These differences might hint at different compatibility levels and strengths of physical interactions of BW on the one hand and pine bark waxes on the other with the two emulsifiers, reflecting their substantially different chemical compositions and polarities.

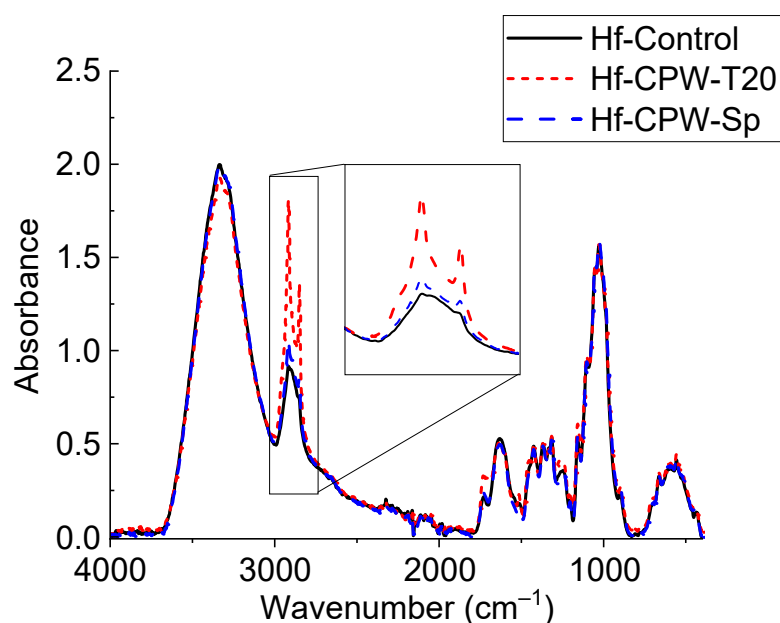


Figure 3. Exemplar FTIR spectra of Hf (control) and Hf coated with CPW-T20 and CPW-Sp emulsions, respectively. The inset shows a magnification of the aliphatic CH stretching region.

For a more quantitative evaluation of the wax coatings, solid state ^{13}C CP/MAS NMR spectroscopy was employed. Exemplar spectra are shown in the Supplementary Materials (Figure S5). From these data, ratios between the integrals for carbon atoms assigned to cellulosic and aliphatic groups (as present in the waxes) were extracted, which are shown in Table 4. The signals from carboxylic acids and related functionalities such as esters which are present in the waxes will have some contribution to the integrated signal assigned to cellulose. However, due to the low weight fraction of the waxes compared to fibres and the low atomic fraction of carboxy-type carbons in the waxes, this effect can be expected to be very minor. Each formulation showed a substantial increase in the aliphatic/cellulosic

carbon ratio compared to the Hf control, confirming that the coating process was successful for all of the emulsions. Comparing the relative increases between the emulsions using the same wax, but with two different emulsifiers, the same trend became evident, as had qualitatively already been observed from FTIR spectroscopy: wax deposition was more effective for CPW and RPW when T20-based emulsions were employed, while coating with BW worked better with Sp.

Table 4. Integrated signals and ratios of carbon atoms corresponding to cellulose and aliphatic (wax) functionalities in uncoated Hf (control) and Hf coated with hydrophobic formulations (measured by solid state ^{13}C CP/MAS NMR).

		Integral (%)	Carbon Ratio (Aliphatic–Cellulosic)	Increase ¹ (%)
Hf-Control	Cellulose	98.76	0.0126	0
	Aliphatic	1.24		
Hf-CPW-T20	Cellulose	97.53	0.0253	102
	Aliphatic	2.47		
Hf-CPW-Sp	Cellulose	97.68	0.0238	89
	Aliphatic	2.32		
Hf-RPW-T20	Cellulose	98.28	0.0299	138
	Aliphatic	1.72		
Hf-RPW-Sp	Cellulose	96.85	0.0233	86
	Aliphatic	3.15		
Hf-BW-T20	Cellulose	97.1	0.0175	39
	Aliphatic	2.90		
Hf-BW-Sp	Cellulose	97.72	0.0325	159
	Aliphatic	2.28		

¹ compared to Hf-Control.

Fluorescence microscopy was employed to visualise the wax distribution on the coated fibres. All three types of waxes showed autofluorescence when excited in the UV range (355 nm), albeit with very different relative intensities (Figure 4a): the strongest emission was obtained from CPW, with a slightly lower response from RPW. Since none of the main constituents of either wax (long chain aliphatic acids and alcohols) are fluorescent, the emission must be caused by minor impurities, such as aromatic compounds derived from lignin, tannin or other polyphenolic bark components [63]. Since their concentration was significantly reduced by the winterisation process, RPW can be expected to be less fluorescent than CPW, which is exactly what was found experimentally. BW exhibited a substantially reduced emission intensity compared to either type of pine bark wax, indicating the almost complete absence of fluorescent moieties. Earlier publications have reported significant levels of autofluorescence from BW; however, direct intensity comparisons with these data are highly challenging, and differences might arise from the measurement conditions (non-identical excitation wavelengths, etc.) or from variations in sources and therefore sample composition [64]. No autofluorescence at all was detected in T20 upon excitation at 355 nm, in line with its chemical structure. By contrast, Sp is known to contain chlorophyll, which is highly fluorescent when excited in the visible range (561 nm was used in this study). Correspondingly, intense emission in the orange-red part of the spectrum was observed from Sp. Due to the different excitation wavelengths, a direct comparison of fluorescence intensities between the waxes and Sp was impossible. Instead, CPW and Sp were both normalised to a maximum emission of one for display in Figure 4a, although it is likely that the emission from Sp was significantly more intense.

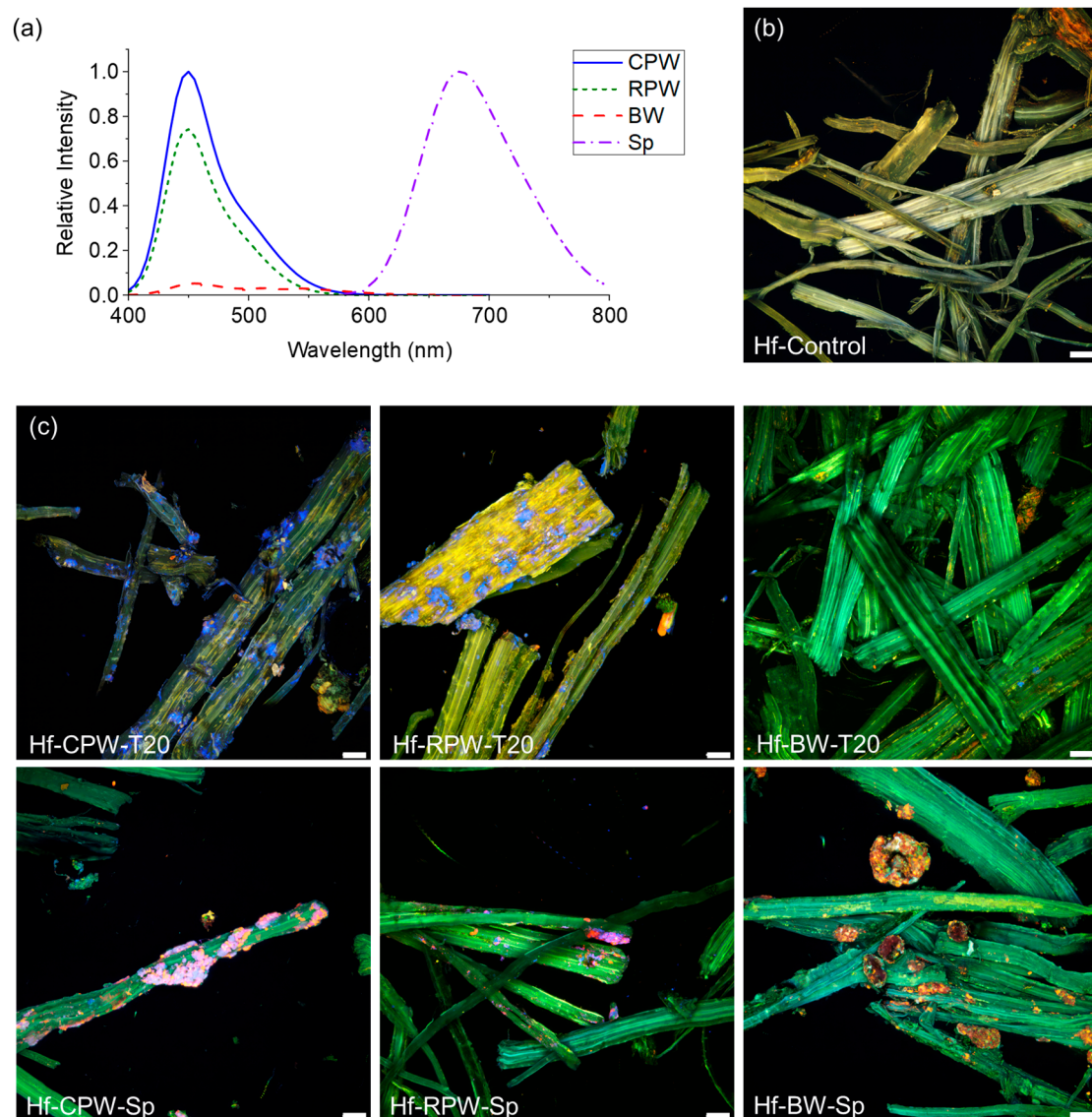


Figure 4. Wax visualisation on the fibres via autofluorescence. (a) Fluorescence spectra for the emulsion components (excitation at 355 nm, except for Sp, where 561 nm light was used). No emission was observed from T20. Relative emission intensities for the waxes were normalised to CPW emission; Sp emission was normalised independently because of the different excitation wavelengths. (b) Confocal fluorescence microscopy of Hf-Control (excitation at 355 nm, emission 400–480 nm). (c) Confocal fluorescence spectroscopy of Hf coated with different emulsions (excitation at 488 nm and 561 nm, emission 500–550 nm and 570–700 nm, respectively). Scalebar = 50 micrometres.

The autofluorescence from the waxes and Sp allowed their detection and visualisation on the fibres via confocal fluorescence microscopy without the use of fluorescent labels. In line with our expectations, the uncoated control (Hf-Control) showed no signs of wax deposition, although it displayed some autofluorescence itself (Figure 4b). This photoemission likely originated from lignin (green), flavonoids (yellow), and tannins (yellow-orange) [65]. By contrast, both CPW and RPW clearly showed up on the fibres due to their blue fluorescence when the non-fluorescent T20 was used as the emulsifier. BW, however, could not be reliably detected in this case because of its too weak emission intensity (Figure 4c, middle row). When Sp was used as the emulsifier, its own orange-red autofluorescence combined with the blue fluorescence of CPW and RPW resulted in a purple colour, while for the BW emulsion, only the Sp emission was visible (Figure 4c, bottom row).

The spatial distribution on the fibres did not reveal significant differences between the waxes; however, there was a clear influence of the emulsifier: when T20 was used, both CPW and RPW were uniformly distributed as regular individual deposits on the fibres; no conclusions about Hf-BW-T20 could be drawn due to the weak emission of the BW. In contrast to the T20-based emulsions, all three emulsions prepared with Sp showed much more clumping and aggregation of the waxes, and the deposits were often detached from the fibres, rather than located on the fibre surfaces. Based on the microscopic fluorescence analyses, using T20 as the emulsifier seemed to result in a more effective coating process, regardless of the pine wax used. Again, this finding supports the spectroscopic observations discussed earlier. No indications were found for the waxes to infiltrate the fibre walls; instead, they remained on the surfaces of the fibres.

TGA analyses were performed on the coated fibres to independently quantify the number of waxes deposited during the dry blending process. However, as shown in the Supplementary Materials (Figure S6), all TGA curves followed the same degradation trend as the uncoated control, independent of the emulsion used. The sensitivity of TGA was clearly insufficient in detecting the low concentrations of wax emulsions deposited on the fibres, as they had already been indicated by ssNMR. However, TGA demonstrated that the coated fibres exhibited sufficient thermal stability to withstand the temperatures applied during compounding with bPBS and during the injection moulding processes (160 °C).

The effect of the wax coatings on the water repellency of the fibres was investigated using time-dependent water contact angle measurements on pads prepared from untreated control fibres and wax-coated fibres (Figure 5). While eventually all of the water droplets were fully absorbed into the pads, the timeframe for these processes was substantially slowed down by applying a hydrophobic coating. Coating-free fibres fully absorbed the water droplets within 15 s, while all samples of coated fibres only showed a reduction in contact angle between 5° and 25°, even after considerably longer times. These findings demonstrate a strong increase in the hydrophobic character and thus the water repellent properties of the hemp fibres upon deposition of the wax emulsions. Similar results have been reported on other types of wax coatings on substrates composed of natural fibres [66,67]. There was some indication of the crude pine wax being slightly less effective than either refined pine wax or beeswax. This is potentially related to a reduction in the contents of more polar components in the pine wax through the winterisation process.

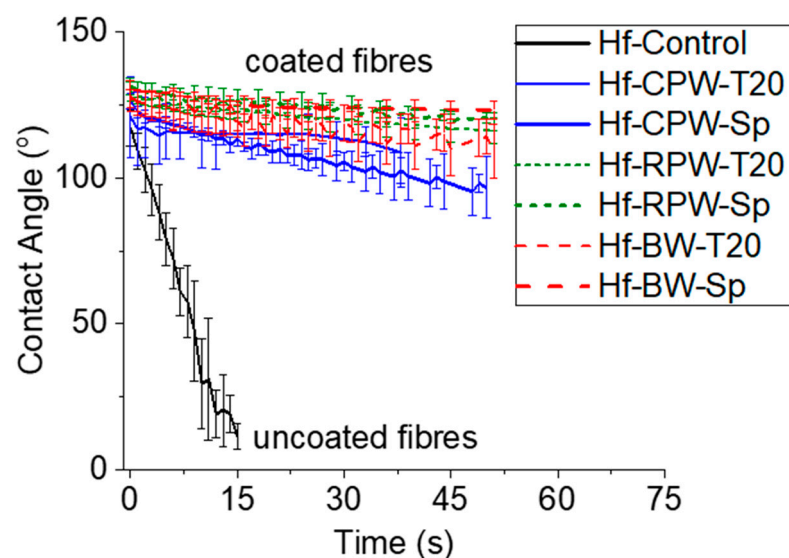


Figure 5. Time-dependent contact angle measurements of water droplets on pads prepared from uncoated hemp fibres (Hf-Control) and hemp fibres coated with different wax emulsions. Error bars represent one standard deviation ($n = 3$).

3.4. Composites

3.4.1. Thermal Characteristics

Pure bPBS showed two endothermic melting transitions in DSC (second heating run) at around 100–120 °C and a single crystallisation peak at 88 °C (Figure 6; Table 5), observations which are in agreement with earlier reports [52]. Based on the melting enthalpy, its crystallinity can be estimated to be about 31% [52,53]. A glass transition at ca. −31 °C was also detected, characteristic of the amorphous fraction. Upon compounding with hemp fibres, the crystallisation peak moved to 80 °C, while no significant changes were observed between the uncoated control fibres and fibres coated with waxes (Figure 6; Table 5; Supplementary Materials, Figures S7–S9; Table S4). Neither the crystallinity nor the glass transition temperature were affected by the addition of Hf. By contrast, the nature of the melting peak qualitatively changed: instead of two endothermic transitions, the composites exhibited a small exothermic peak (at ca. 103 °C), followed by a much stronger endothermic peak (at ca. 114 °C), independent of the nature of the fibre coating. This hints at a relaxation of the stresses in the bPBS which have built up due to the incorporation of the fibre material. A similar thermal behaviour was reported earlier for bPBS compounded with grape pomace [53].

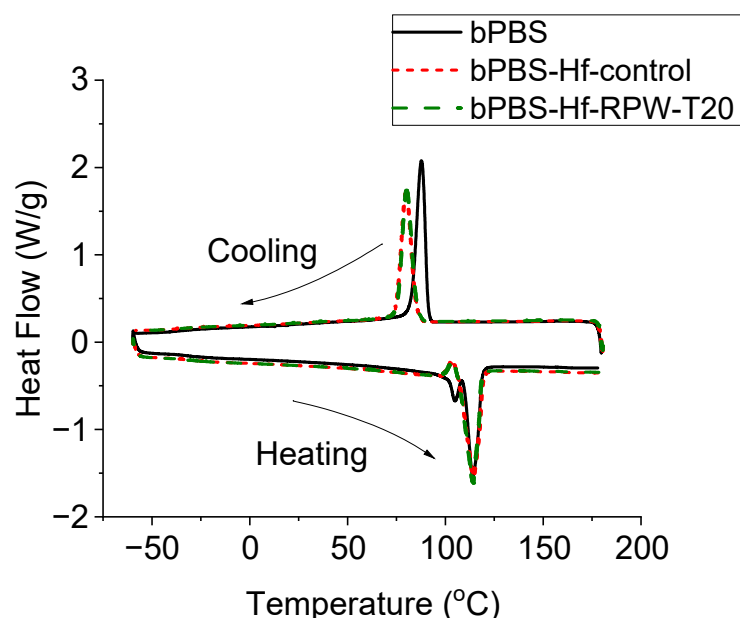


Figure 6. DSC thermograms of bPBS and its composites with untreated Hf and Hf coated with RPW-T20 emulsion (cooling run and second heating run; exo up).

Table 5. Thermal properties of bPBS and its composites with Hf (coated and uncoated), as determined by DSC. Shown here are results from the second heating ramp. Experimental uncertainties are reported as one standard variation ($n = 3$).

	Glass Transition (°C)	Melting Enthalpy (J/g)	Crystallinity (%)	Peak Maximum (°C)
bPBS	-31.5 ± 0.2	61.9 ± 1.6	30.9 ± 0.8	113.9 ± 0.1
bPBS-Hf-Control	-32.9 ± 1.2	54.6 ± 0.6	30.3 ± 0.3	113.9 ± 0.1
bPBS-Hf-CPW-T20	-31.9 ± 0.7	53.2 ± 0.5	29.5 ± 0.3	114.0 ± 0.1
bPBS-Hf-CPW-Sp	-31.8 ± 0.1	52.0 ± 0.3	28.9 ± 0.2	113.8 ± 0.1
bPBS-Hf-RPW-T20	-32.9 ± 0.7	53.0 ± 0.7	29.5 ± 0.4	113.9 ± 0.1
bPBS-Hf-RPW-Sp	-32.9 ± 0.9	54.4 ± 0.8	30.3 ± 0.5	114.0 ± 0.1
bPBS-Hf-BW-T20	-32.4 ± 0.2	52.9 ± 0.5	29.4 ± 0.3	113.8 ± 0.1
bPBS-Hf-BW-Sp	-33.5 ± 1.0	52.8 ± 0.7	29.3 ± 0.4	113.8 ± 0.1

3.4.2. Mechanical Performance

Other authors have previously shown that wax coatings are able to improve the compatibility between natural fibres and polymer matrices and can thus lead to enhanced mechanical performances [9,10,13]. Therefore, tensile, flexural, and impact strength testing was performed on the composites (Figure 7a–c; Supplementary Materials, Figure S10). While the effects of fibre addition on the mechanical properties were obvious, no further change was measured if the fibres were coated, regardless of the type of wax and the emulsifier used. This finding is in disagreement with the results of Gigante et al., who found significant effects of natural wax coatings when investigating composites of PLA/PBS blends or PHBV with rice and wheat bran fillers [13,45]. For the materials systems used in the current study, tensile testing showed a moderate reduction in maximum tensile stress (by ca. 15%) and almost a doubling in Young's modulus when any type of Hf (coated or uncoated control) was added to bPBS. The increase in Young's modulus indicates that the presence of the fibres made the composites much stiffer than the neat bPBS matrix, which can be highly desirable depending on the intended application. The strain at break of bPBS dropped by more than an order of magnitude upon compounding with Hf. However, no substantial variation was found between composites prepared using coated or uncoated fibres, independent of the formulation used. The electron microscopic imaging of the transverse fracture profiles looked very similar for the control samples and the composites prepared with wax-coated fibres (Figure 7d). In all cases, the fibres had clearly been pulled out of the polymer matrix; this detachment is indicative of a weak adhesion between the Hf surfaces and the bPBS polymer matrix, which is why no improvement in their mechanical behaviour was observed.

Flexural and impact testing gave a very similar picture as tensile testing: substantial differences were only found between pure bPBS and the composites, but not different types of fibres (Supplementary Materials, Figure S10). A small, yet significant, reduction in both the maximum flexural stress and modulus was observed when uncoated control fibres were replaced by coated ones. While this effect was too weak to have practical implications for potential applications, it did hint at a possible explanation for the absence of strong effects of the waxes. The bPBS, being a rather hydrophobic material, has a high affinity for the likewise very non-polar waxes. These are therefore likely to detach from the fibre surface and dissolve into the polymer matrix during compounding. Being stripped of their wax coating, the compatibility between the fibres and the polymer matrix was therefore not improved compared to uncoated Hf. Natural wax addition at substantial levels (up to 15% by weight) has been demonstrated to influence the mechanical properties of aliphatic biopolyesters significantly [46]. However, due to their low concentration in the bPBS, the pine waxes used in the current study cannot be expected to exert strong effects on the mechanical properties of the matrix, beyond a slight plasticising effect under flexural testing. By contrast, Gigante et al. used a more polar matrix (due to the significant percentage of PLA with a lower content of aliphatic moieties than bPBS), which was less likely to remove the waxes from the surface of the bran platelets that were used in their study [45]. Another potential explanation for the discrepancies between their findings and the results presented here might be the differences in filler particles size, shape, aspect ratio and chemical composition, and the different coating method used [13].

An overview of earlier reports using similar concepts and materials systems, and a comparison of their outcomes with those of this study, is presented as Table S5 in the Supplementary Materials. From these sources, it becomes evident that often higher weight fractions of coating materials are deposited on the fibres than the 2–3 wt% used here. Increasing the wax content on the hemp fibres could thus potentially offer an alternative route to achieve stronger effects on the mechanical properties of the composites.

The hydrophobicity of natural waxes has been shown to depend on the deposition conditions, such as temperature and solvent composition [68]. Another method to decrease the hydrophobicity of waxes is the introduction of polar chemical functionalities through controlled oxidation [69]. Adjusting the surface properties of the pine waxes through either

variations in coating conditions or oxidation degree therefore could offer additional options to prevent dissolution into the polymer matrix. In this way, the waxes might remain attached to the fibres during compounding with bioPBS, thus improving fibre–matrix interactions and ultimately, composite performance.

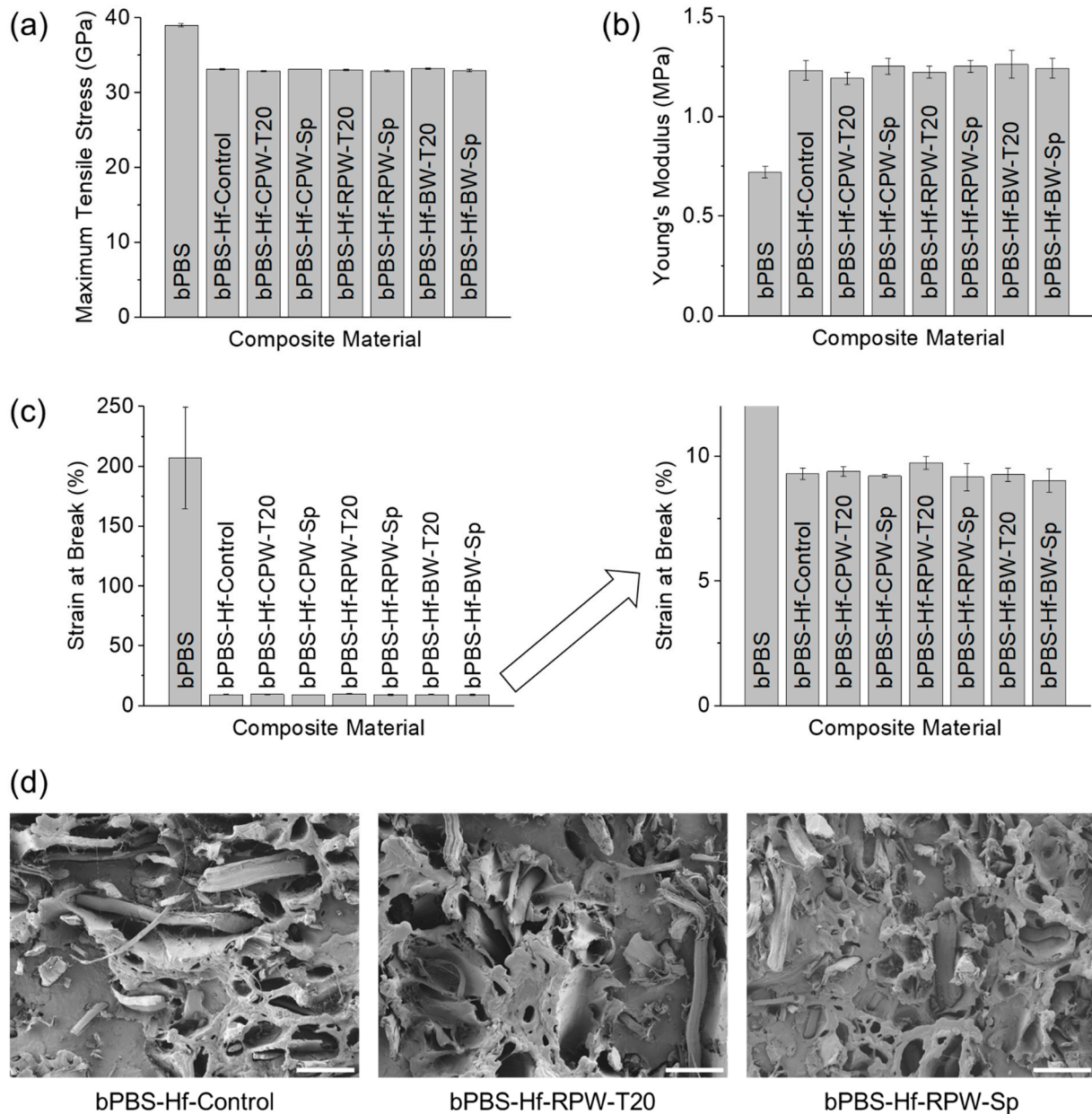


Figure 7. Tensile testing for bPBS and its composites with Hf. (a) Maximum tensile stress, (b) Young's modulus, (c) strain at break (displayed at two different scales for clarity). Error bars indicate one standard deviation. (d) Electron microscopic images of the fracture surfaces of three exemplar composites. Scale bar = 200 micrometres.

4. Conclusions

Natural fibres, specifically hemp fibres (Hf), have been successfully coated with hydrophobic compounds originating from *P. radiata* bark and with beeswax, using a dry blending process. A combination of spectroscopic and microscopic techniques was used to characterise the coated fibres and to quantify their contents of hydrophobic compounds. Due to the inherent autofluorescence of Sp and certain components in the pine bark waxes,

confocal fluorescence microscopy was found to be an excellent tool to visualise the spatial distribution of these waxes on the fibre surfaces. Depending on their composition and the photoluminescence characteristics of their individual components, different emulsions displayed variations in emission colours. This phenomenon offered the possibility to distinguish different wax formulations from one another. T20-based emulsions produced a more homogeneous wax coating on the fibres, while Sp-based emulsions displayed significant aggregation. By contrast, no significant influences of the different wax types on the coating quality were observed.

Both the emulsions and the coated fibres exhibited sufficient thermal stability in order to be suitable for compounding with bio-based poly(butylene succinate) (bPBS) and the injection moulding of the resulting fibre-reinforced composites. The addition of 10 wt% of Hf into the polymer matrix had substantial effects on the mechanical properties of these composite materials, most prominently causing an increase in Young's modulus and a drastic reduction in strain at break. However, no meaningful differences in mechanical behaviour were observed between the composites prepared from coated or uncoated fibres. This observation was attributed to the dissolution of wax coatings from the fibre surfaces into the bPBS matrix during compounding. In systems with different polymer matrices, however, the presence of natural waxes on the surfaces of Hf can be expected to have beneficial effects on their compatibility with the polymer, and therefore ultimately on their mechanical performances. Judging from a comparison with earlier work, increasing the wax load on the fibres might offer another approach to achieve improved composite properties. Alternatively, optimised wax deposition conditions or a controlled oxidation of the waxes might have similar beneficial effects.

Supplementary Materials: The following supporting information can be downloaded at <https://www.mdpi.com/article/10.3390/fib12110096/s1>, Table S1: Chemical analysis of untreated hemp fibres; Table S2: DSC heat-cool-heat programs for starting materials, emulsions and composites; Table S3: Degradation transitions, with corresponding temperature and weight loss percentage under nitrogen atmosphere for the dried emulsions; Table S4: Thermal transitions for the composite materials obtained by DSC; Table S5: Comparison of outcomes of the current study with earlier reports on similar materials systems (polymer composites reinforced with coated hemp fibres); Figure S1: DSC thermograms of CPW and its emulsions with T20 and Sp; Figure S2: DSC thermograms of RPW and its emulsions with T20 and Sp; Figure S3: DSC thermograms of BW and its emulsions with T20 and Sp; Figure S4: FTIR spectra of starting materials, CPW formulations, BW formulations, and RPW formulations; Figure S5: Exemplar ¹³C CP/MAS NMR spectra of untreated Hf, RPW, and Hf coated with either RPW-T20 or RPW-Sp emulsions; Figure S6: Thermal degradation behaviour (determined by TGA) of Hf fibres coated with different wax formulations, and uncoated control; Figure S7: DSC thermograms of bPBS and its composites with untreated Hf and Hf coated with RPW-Sp emulsion; Figure S8: DSC thermograms of bPBS and its composites with untreated Hf and Hf coated with CPW-T20 and CPW-Sp emulsions; Figure S9: DSC thermograms of bPBS and its composites with untreated Hf and Hf coated with BW-T20 and CPW-Sp emulsions; Figure S10: Mechanical performance comparison of bPBS and its composites with coated and uncoated Hf (flexural and impact testing).

Author Contributions: Conceptualisation, R.R.; methodology, R.A., R.R., M.N. and L.D.; validation, R.A. and R.R.; formal analysis, R.A., R.R., M.N., L.D. and J.H.B.; investigation, M.N., L.D., C.B., C.M.-L., J.H.B., A.T., A.D., R.M., J.H. and J.B.; resources, R.A., A.D. and S.H.; data curation, R.A. and R.R.; writing—original draft preparation, R.A., R.R., M.N. and L.D.; writing—review and editing, R.A., R.R., L.D., C.B., C.M.-L., J.H.B., A.D., J.B. and S.H.; visualisation, R.A., L.D. and J.H.B.; supervision, R.A. and R.R.; project administration, R.A., A.D. and S.H.; funding acquisition, S.H. All authors have read and agreed to the published version of the manuscript.

Funding: Funding for this work has been received from New Zealand's Ministry of Business, Innovation and Employment through the Endeavour programme Bark Biorefinery: Unlocking new hydrophobic polymers (C04X1802) and through the Strategic Science Investment Fund (C04X1703) via the Bark Based Bioproducts project. Part of this research has been conducted under the umbrella of the Scion—INRAE—Université de Montpellier—Institut Agro Associated International Laboratory

BIOMATA collaboration and has been carried out within the SMARTPOP project funded by H2020-EU-MSCA-IF (grant number 893040).

Data Availability Statement: The raw data supporting the conclusions of this article will be made available by the authors on request.

Acknowledgments: The authors are grateful to Michael Robertson (Scion) for his support with GC-MS sample preparation and data acquisition, to Sunita Patel (Scion) for the chemical analysis of the hemp fibres, and to Robin Parr (Scion) for water absorption tests. Maxime Barbier (Scion) and Dr Angeliq Greene (Scion) are acknowledged for their internal review of the manuscript prior to submission. Nick Lambert's (Scion) support with preparing the graphical abstract is kindly acknowledged, too.

Conflicts of Interest: The authors declare no conflicts of interest. The funders had no role in the design of the study; in the collection, analyses, or interpretation of data; in the writing of the manuscript; or in the decision to publish the results.

References

1. Kanokpanont, S.; Damrongsakkul, S.; Ratanavaraporn, J.; Aramwit, P. Physico-chemical properties and efficacy of silk fibroin fabric coated with different waxes as wound dressing. *Int. J. Biol. Macromol.* **2013**, *55*, 88–97. [[CrossRef](#)] [[PubMed](#)]
2. Abbass, A.; Paiva, M.C.; Oliveira, D.V.; Lourenço, P.B.; Fangueiro, R.; Alves, N.M. The Potential of Beeswax Colloidal Emulsion/Films for Hydrophobization of Natural Fibers Prior to NTRM Manufacturing. *Key Engin. Mater.* **2022**, *916*, 82–90. [[CrossRef](#)]
3. Forsman, N.; Lozhechnikova, A.; Khakalo, A.; Johansson, L.S.; Vartiainen, J.; Österberg, M. Layer-by-layer assembled hydrophobic coatings for cellulose nanofibril films and textiles, made of polylysine and natural wax particles. *Carbohydr. Polym.* **2017**, *173*, 392–402. [[CrossRef](#)] [[PubMed](#)]
4. Forsman, N.; Johansson, L.S.; Koivula, H.; Tuure, M.; Kääriäinen, P.; Österberg, M. Open coating with natural wax particles enable scalable, non-toxic hydrophobation of cellulose-based textiles. *Carbohydr. Polym.* **2020**, *227*, 115363. [[CrossRef](#)]
5. Bachchan, A.A.; Das, P.P.; Chaudhary, V. Effect of moisture absorption on the properties of natural fiber reinforced polymer composites: A review. *Mater. Today Proc.* **2022**, *49*, 3403–3408. [[CrossRef](#)]
6. Zwawi, M. A review on natural fiber bio-composites, surface modifications and applications. *Molecules* **2021**, *26*, 404. [[CrossRef](#)]
7. Nurazzi, N.; Harussani, M.M.; Aisya, H.A.; Ilyas, R.A.; Norrrahim, M.N.F.; Khalina, A.; Abdulla, N. Treatments of natural fiber as reinforcement in polymer composites—A short review. *Funct. Comp. Struct.* **2021**, *3*, 024002. [[CrossRef](#)]
8. Qaiss, A.E.K.; Bouhfid, R.; Essabir, H. Natural fibers reinforced polymeric matrix: Thermal, mechanical and interfacial properties. In *Biomass and Bioenergy: Processing and Properties*; Hakeem, K.R., Jawaid, M., Rashid, U., Eds.; Springer International Publishing: Cham, Switzerland, 2014; Volume 1, pp. 225–245.
9. Nhlapo, L.; Luyt, A. Thermal and mechanical properties of LDPE/sisal fiber composites compatibilized with functionalized paraffin waxes. *J. Appl. Polym. Sci.* **2012**, *123*, 3627–3634. [[CrossRef](#)]
10. Atthikumar, N.; Kannakumar, K.; Kanakarajan, P.; Sathishkumar, S.; Augustin Santhiyagu, I.; Hasane Ahammad, S. Investigation of the thermal and mechanical behavior of recycled low-density polyethylene/Hemp fiber composites containing paraffin wax. *Mater. Today Proc.* **2023**, *in press*. [[CrossRef](#)]
11. Floros, M.C.; Raghunanan, L.; Narine, S.S. A toolbox for the characterization of biobased waxes. *Eur. J. Lipid Sci. Technol.* **2017**, *119*, 1600360. [[CrossRef](#)]
12. Fratini, F.; Cilia, G.; Turchi, B.; Felicioli, A. Beeswax: A minireview of its antimicrobial activity and its application in medicine. *Asian Pac. J. Trop. Med.* **2016**, *9*, 839–843. [[CrossRef](#)] [[PubMed](#)]
13. Gigante, V.; Cinelli, P.; Righetti, M.C.; Sandroni, M.; Polacco, G.; Seggiani, M.; Lazzeri, A. On the use of biobased waxes to tune thermal and mechanical properties of polyhydroxyalkanoates-bran biocomposites. *Polymers* **2020**, *12*, 2615. [[CrossRef](#)] [[PubMed](#)]
14. Sobol, L.; Sabat, D.; Dyjakon, A. Assessment of Bark Properties from Various Tree Species in Terms of Its Hydrophobicity and Energy Suitability. *Energies* **2023**, *16*, 6586. [[CrossRef](#)]
15. Huang, Z.; Yan, N. Characterization of major components in barks from five Canadian tree species. *Wood Fiber Sci.* **2014**, *46*, 167–174.
16. Sandoval-Rivas, D.; Moczko, E.; Morales, D.V.; Hepp, M.I. Evaluation and characterization of a new method of extracting bark wax from *Pinus radiata* D. Don. *Ind. Crops Prod.* **2021**, *174*, 114161. [[CrossRef](#)]
17. Sandoval-Rivas, D.; Morales, D.V.; Hepp, M.I. Toxicity evaluation of *Pinus radiata* D. Don bark wax for potential cosmetic application. *Food Chem. Toxicol.* **2023**, *178*, 113896. [[CrossRef](#)]
18. Bento, A.; Escórcio, R.; Tomé, A.S.; Robertson, M.; Gaugler, E.C.; Malthus, S.J.; Raymond, L.G.; Hill, S.J.; Silva Pereira, C. *Pinus radiata* bark sequentially processed using scCO₂ and an ionic liquid catalyst yields plentiful resin acids and alkanolic acids enriched suberin. *Ind. Crops Prod.* **2022**, *185*, 115172. [[CrossRef](#)]
19. Quilter, H.C.; Risani, R.; Gallagher, S.; Robertson, M.; Thumm, A.; Thomas, H.P.; Abbel, R. Synthesis of hydrophobic biopolyesters from depolymerized *Pinus radiata* bark suberin. *Holzforschung* **2024**, *78*, 303–316. [[CrossRef](#)]

20. Rogers, D.L. In situ genetic conservation of a naturally restricted and commercially widespread species, *Pinus radiata*. *For. Ecol. Manag.* **2004**, *197*, 311–322. [[CrossRef](#)]
21. Nixon, C.; Gamperle, D.; Pambudi, D.; Clough, P. *Plantation forestry statistics: Contribution of forestry to New Zealand*; New Zealand Institute of Economic Research: Wellington, New Zealand, 2017; p. 14.
22. Chen, H.; Chauhan, P.; Yan, N. “Barking” up the right tree: Biorefinery from waste stream to cyclic carbonate with immobilization of CO₂ for non-isocyanate polyurethanes. *Green Chem.* **2020**, *22*, 6874–6888. [[CrossRef](#)]
23. Alonso-Esteban, J.I.; Caroch, M.; Barros, D.; Velho, M.V.; Heleno, S.; Barros, L. Chemical composition and industrial applications of Maritime pine (*Pinus pinaster* Ait.) bark and other non-wood parts. *Rev. Environ. Sci. Bio.* **2022**, *21*, 583–633. [[CrossRef](#)]
24. Passialis, C.N.; Voulgaridis, E.V. Water repellent efficiency of organic solvent extractives from Aleppo pine leaves and bark applied to wood. *Holzforschung* **1999**, *53*, 151–155. [[CrossRef](#)]
25. Manaia, J.P.; Manaia, A.T.; Rodrigues, L. Industrial hemp fibers: An overview. *Fibers* **2019**, *7*, 106. [[CrossRef](#)]
26. Promhuad, K.; Srisa, A.; San, H.; Laorenza, Y.; Wongphan, P.; Sodsai, J.; Tansin, K.; Phromphen, P.; Chartvivatpornchai, N.; Ngoenchai, P.; et al. Applications of Hemp Polymers and Extracts in Food, Textile and Packaging: A Review. *Polymers* **2022**, *14*, 4274. [[CrossRef](#)]
27. Ingrao, C.; Giudice, A.L.; Bacenetti, J.; Tricase, C.; Dotelli, G.; Fiala, M.; Siracusa, V.; Mbohwa, C. Energy and environmental assessment of industrial hemp for building applications: A review. *Renew. Sust. Energy Rev.* **2015**, *51*, 29–42. [[CrossRef](#)]
28. Mohanty, A.; Tummala, P.; Liu, W.; Misra, M.; Mulukutla, P.V.; Drzal, L.T. Injection molded biocomposites from soy protein based bioplastic and short industrial hemp fiber. *J. Polym. Environ.* **2005**, *13*, 279–285. [[CrossRef](#)]
29. Wróbel-Kwiatkowska, M.; Czemplik, M.; Kulma, A.; Żuk, M.; Kaczmar, J.; Dymińska, L.; Hanuza, J.; Ptak, M.; Szopa, J. New biocomposites based on bioplastic flax fibers and biodegradable polymers. *Biotechnol. Prog.* **2012**, *28*, 1336–1346. [[CrossRef](#)]
30. Tanasá, F.; Zănoagă, M.; Teacă, C.A.; Nechifor, M.; Shahzad, A. Modified hemp fibers intended for fiber-reinforced polymer composites used in structural applications—A review. I. Methods of modification. *Polym. Comp.* **2020**, *41*, 5–31. [[CrossRef](#)]
31. Song, Y.S.; Lee, J.T.; Ji, D.S.; Kim, M.W.; Lee, S.H.; Youn, J.R. Viscoelastic and thermal behavior of woven hemp fiber reinforced poly(lactic acid) composites. *Comp. Part B Engin.* **2012**, *42*, 856–860. [[CrossRef](#)]
32. Song, Y.; Liu, J.; Chen, S.; Zheng, Y.; Ruan, S.; Bin, Y. Mechanical Properties of Poly(Lactic Acid)/Hemp Fiber Composites Prepared with a Novel Method. *J. Polym. Environ.* **2013**, *21*, 1117–1127. [[CrossRef](#)]
33. Kremensas, A.; Kairyte, A.; Vaitkus, S.; Vėjelis, S.; Balčiūnas, G. Mechanical Performance of Biodegradable Thermoplastic Polymer-Based Biocomposite Boards from Hemp Shivs and Corn Starch for the Building Industry. *Materials* **2019**, *12*, 845. [[CrossRef](#)] [[PubMed](#)]
34. Gill, A.R.; Boveys, B.R.; Cavagnaro, T.R.; Burton, R.A. The potential of industrial hemp (*Cannabis sativa* L.) as an emerging drought resistant fibre crop. *Plant Soil* **2023**, *493*, 7–16. [[CrossRef](#)]
35. Chawla, R.; Fang, Z. Hemp macromolecules: Crafting sustainable solutions for food and packaging innovation. *Int. J. Biol. Macromol.* **2024**, *273*, 132823. [[CrossRef](#)] [[PubMed](#)]
36. De Costa Santos, A.C.; Archbold, P. Suitability of Surface-Treated Flax and Hemp Fibers for Concrete Reinforcement. *Fibers* **2022**, *10*, 101. [[CrossRef](#)]
37. Lawan, I.; Qiang, L.; Zhou, W.; Yi, J.; Song, J.; Zhang, M.; Huang, Z.; Pang, J.; Yuan, Z. Modifications of hemp twine for use as a fiber in cement composite: Effects of hybrid treatments. *Cellulose* **2018**, *25*, 2009–2020. [[CrossRef](#)]
38. Fuller, G.T.; Considine, T.; MacGibbon, A.; Golding, M.; Matia-Merino, L. Effect of Tween emulsifiers on the shear stability of partially crystalline oil-in-water emulsions stabilized by sodium caseinate. *Food Biophys.* **2018**, *13*, 80–90. [[CrossRef](#)]
39. Silva, S.C.; Almeida, T.; Colucci, G.; Santamaria-Echart, A.; Manrique, Y.A.; Dias, M.M.; Barros, L.; Fernandes, A.; Colla, E.; Filomena Barreiro, M. Spirulina (*Arthrospira platensis*) protein-rich extract as a natural emulsifier for oil-in-water emulsions: Optimization through a sequential experimental design strategy. *Colloids Surf. A Physicochem. Eng. Asp.* **2022**, *648*, 129264. [[CrossRef](#)]
40. Petersen, S.; Ulrich, J. Effectiveness of Polyoxyethylene Nonionic Emulsifiers in Emulsification Processes Using Disc Systems. *Chem. Engin. Technol.* **2011**, *34*, 1869–1875. [[CrossRef](#)]
41. Park, J.-Y.; Choi, M.J.; Yu, H.; Choi, Y.; Park, K.M.; Chang, P.S. Multi-functional behavior of food emulsifier erythorbyl laurate in different colloidal conditions of homogenous oil-in-water emulsion system. *Colloids Surf. A Physicochem. Eng. Asp.* **2022**, *636*, 128127. [[CrossRef](#)]
42. Kamaruding, N.A.; Muhammad Daud, N.A.; Ismail, N.; Shaharuddin, S. Effect of Different Solubilization pH Values on the Functional Properties of Protein Spirulina platensis Isolated Through Acidic Precipitation. *J. Aquat. Food Prod. Technol.* **2022**, *31*, 1025–1037. [[CrossRef](#)]
43. Paswan, M.B.; Chudasama, M.M.; Mitra, M.; Bhayani, K.; George, B.; Chatterjee, S.; Mishra, S. Fluorescence Quenching Property of C-Plyocyanin from Spirulina platensis and its Binding Efficacy with Viable Cell Components. *J. Fluoresc.* **2016**, *26*, 577–583. [[CrossRef](#)] [[PubMed](#)]
44. Loxton, C.; Thumm, A.; Grigsby, W.J.; Adams, T.A.; Ede, R.M. Resin distribution in medium density fiberboard. Quantification of UF resin distribution on blowline-and dry-blended MDF fiber and panels. *Wood Fiber Sci.* **2003**, *35*, 370–380.
45. Gigante, V.; Aliotta, L.; Canesi, I.; Sandroni, M.; Lazzeri, A.; Coltelli, M.B.; Cinelli, P. Improvement of interfacial adhesion and thermomechanical properties of PLA based composites with wheat/rice bran. *Polymers* **2022**, *14*, 3389. [[CrossRef](#)] [[PubMed](#)]

46. Mendoza-Duarte, M.E.; Estrada-Moreno, I.A.; López-Martínez, E.I.; Vega-Rios, A. Effect of the Addition of Different Natural Waxes on the Mechanical and Rheological Behavior of PLA—A Comparative Study. *Polymers* **2023**, *15*, 305. [[CrossRef](#)]
47. Ouakarrouch, M.; Bousshine, S.; Bybi, A.; Laaroussi, N.; Garoum, M. Acoustic and thermal performances assessment of sustainable insulation panels made from cardboard waste and natural fibers. *Appl. Acoust.* **2022**, *199*, 109007. [[CrossRef](#)]
48. Chungsiriporn, J.; Khunthongkaew, P.; Wongnoipla, Y.; Sopajarn, A.; Karrila, S.; Lewkittayakorn, J. Fibrous packaging paper made of oil palm fiber with beeswax-chitosan solution to improve water resistance. *Ind. Crops Prod.* **2022**, *177*, 114541. [[CrossRef](#)]
49. Khan, A.; Nadeem, M.; Imran, M.; Khalique, A. Impact of winterization on fatty acids' composition, isomers, and oxidative stability of conjugated linoleic acids produced from selected vegetable oils. *J. Food Process. Preserv.* **2021**, *45*, e15254. [[CrossRef](#)]
50. Mayer-Laigle, C.; Beaugrand, J.; Bourmaud, A.; Brionne, L.; Colinart, T.; Dervaux, S.; Fabre, C.; le Guen, M.J.; Korschak, K.; Paës, G.; et al. Datasets on the production routes and the properties of plant powders for manufacturing of green products. *Data in Brief* **2024**, *56*, 110787. [[CrossRef](#)]
51. *International Standard ISO 527-2:2012(E)*; Plastics—Determination of Tensile Properties—Part 2: Test Conditions for Moulding and Extrusion Plastics. International Organization for Standardization: Geneva, Switzerland, 2012.
52. Chen, R.-Y.; Zou, W.; Zhang, H.C.; Zhang, G.Z.; Yang, Z.T.; Jin, G.; Qu, J.P. Thermal behavior, dynamic mechanical properties and rheological properties of poly (butylene succinate) composites filled with nanometer calcium carbonate. *Polym. Test.* **2015**, *42*, 160–167. [[CrossRef](#)]
53. Gowman, A.; Wang, T.; Rodriguez-Uribe, A.; Mohanty, A.K.; Misra, M. Bio-poly (butylene succinate) and its composites with grape pomace: Mechanical performance and thermal properties. *ACS Omega* **2018**, *3*, 15205–15216. [[CrossRef](#)]
54. *International Standard ASTM D790-17*; Standard Test Method for Flexural Properties of Unreinforced and Reinforced Plastics and Electrical Insulating Materials. ASTM International: West Conshohocken, PE, USA, 2017.
55. *International Standard ISO 180:2023*; Plastics—Determination of Izod Impact Strength. International Organization for Standardization: Geneva, Switzerland, 2023.
56. Buchwald, R.; Breed, M.D.; Greenberg, A.R. The thermal properties of beeswaxes: Unexpected findings. *J. Exp. Biol.* **2008**, *211*, 121–127. [[CrossRef](#)] [[PubMed](#)]
57. Dobrosielska, M.; Dobrucka, R.; Kozera, P.; Brząkalski, D.; Gabriel, E.; Głowacka, J.; Jałbrzykowski, M.; Kurzydłowski, K.J.; Przekop, R.E. Beeswax as a natural alternative to synthetic waxes for fabrication of PLA/diatomaceous earth composites. *Sci. Rep.* **2023**, *13*, 1161. [[CrossRef](#)] [[PubMed](#)]
58. Jankauskienė, Z.; Butukė, B.; Gruzdevienė, E.; Cesevičienė, J.; Fernando, A.L. Chemical composition and physical properties of dew- and water retted hemp fibres. *Ind. Crops Prod.* **2015**, *74*, 206–211. [[CrossRef](#)]
59. Larrosa, A.P.Q.; Camara, Á.S.; Pohndorf, R.S.; da Rocha, S.F.; Pinto, L.A.A. Physicochemical, biochemical, and thermal properties of *Arthrospira* (Spirulina) biomass dried in spouted bed at different conditions. *J. Appl. Phycol.* **2018**, *30*, 1019–1029. [[CrossRef](#)]
60. Borriello, A.; Miele, N.A.; Masi, P.; Aiello, A.; Cavella, S. Effect of fatty acid composition of vegetable oils on crystallization and gelation kinetics of oleogels based on natural wax. *Food Chem.* **2022**, *375*, 131805. [[CrossRef](#)]
61. Qiyuan, L.; Jinmei, D.; Ruguang, L.; Chenggong, C.; Yangyuanxiang, X.; Jing, W.; Weixin, Z.; Derong, W.; Shengxia, A. Preparation and properties of fatty acid/alcohol composite phase change mortar. *Constr. Build. Materials* **2024**, *416*, 135195. [[CrossRef](#)]
62. Shi, K.; Liu, G.; Sun, H.; Yang, B.; Weng, Y. Effect of biomass as nucleating agents on crystallization behavior of polylactic acid. *Polymers* **2022**, *14*, 4305. [[CrossRef](#)]
63. Donaldson, L.A. Localizing Molecules in Plant Cell Walls Using Fluorescence Microscopy. In *Histochemistry of Single Molecules: Methods and Protocols*, 2nd ed.; Pellicciari, C., Biggiogera, M., Malatesta, M., Eds.; Springer Nature: New York, NY, USA, 2022; pp. 243–259.
64. Dal Fovo, A.; Mattana, S.; Chaban, A.; Quintero Balbas, D.; Lagarto, J.L.; Striova, J.; Cicchi, R.; Fontana, R. Fluorescence lifetime phasor analysis and Raman spectroscopy of pigmented organic binders and coatings used in artworks. *Appl. Sci.* **2021**, *12*, 179. [[CrossRef](#)]
65. Isidore, E.; Karim, H.; Ioannou, I. Extraction of phenolic compounds and terpenes from *Cannabis sativa* L. by-products: From conventional to intensified processes. *Antioxidants* **2021**, *10*, 942. [[CrossRef](#)]
66. Lee, E.J.; Lim, K.-H. Preparation of eco-friendly wax-coated paper and its rheological and water-resistance characteristics. *Korean J. Chem. Eng.* **2021**, *38*, 2479–2492. [[CrossRef](#)]
67. Chen, C.; Chen, J.; Zhang, S.; Cao, J.; Wang, W. Forming textured hydrophobic surface coatings via mixed wax emulsion impregnation and drying of poplar wood. *Wood Sci. Technol.* **2020**, *54*, 421–439. [[CrossRef](#)]
68. Dent, F.J.; Tyagi, G.; Esat, F.; Cabral, J.T.; Khodaparast, S. Tuneable Topography and Hydrophobicity Mode in Biomimetic Plant-Based Wax Coatings. *Adv. Funct. Mater.* **2024**, *34*, 2307977. [[CrossRef](#)]
69. Salimi, A.; Mirabedini, M.; Atai, M.; Mohseni, M. Studies on the Mechanical Properties and Practical Coating Adhesion of PP Modified by Oxidized Wax. *J. Adh. Sci. Technol.* **2010**, *24*, 1113–1129. [[CrossRef](#)]

Disclaimer/Publisher's Note: The statements, opinions and data contained in all publications are solely those of the individual author(s) and contributor(s) and not of MDPI and/or the editor(s). MDPI and/or the editor(s) disclaim responsibility for any injury to people or property resulting from any ideas, methods, instructions or products referred to in the content.